

Modification of turbulent transport with continuous variation of flow shear in the Large Plasma Device

D.A. Schaffner,¹ T.A. Carter,¹ G.D. Rossi,² D.S. Guice,¹ J.E. Maggs,¹ S. Vincena,¹ and B. Friedman¹

*¹Department of Physics and Astronomy,
University of California, Los Angeles*

²Department of Physics, University of Texas, Austin

(Dated: August 2, 2012)

Abstract

Continuous control over azimuthal flow and shear in the edge of the Large Plasma Device (LAPD) has been achieved using a biasable limiter which has allowed a careful study of the effect of flow shear on pressure-gradient-driven turbulence and transport in LAPD. LAPD rotates spontaneously in the ion diamagnetic direction (IDD); positive limiter bias first reduces, then minimizes (producing a near-zero shear state), and finally reverses the flow into the electron diamagnetic direction (EDD). Degradation of particle confinement is observed in the minimum shearing state and reduction in turbulent particle flux is observed with increasing shearing in both flow directions. Near-complete suppression of turbulent particle flux is observed for shearing rates comparable to the turbulent autocorrelation rate measured in the minimum shear state. Turbulent flux suppression is dominated by amplitude reduction in low-frequency ($< 10\text{kHz}$) density fluctuations. An increase in fluctuations for the highest shearing states is observed with the emergence of a coherent mode which does not lead to net particle transport. The variations of density fluctuations are fit well with power-laws and compare favorably to simple models of shear suppression of transport.

While flow shear does provide a source of free energy for instability and turbulence, it can lead to stabilization of pressure-gradient-driven instabilities and a reduction of turbulent transport in magnetized plasmas [1, 2]. The transport barrier in the high-confinement mode, or H-mode, of tokamak operation [3, 26] is attributed to the spontaneous development of an edge flow layer in which strong shearing suppresses transport [1, 2]. The direct connection between the H-mode edge flow layer and improved confinement was first established in experiments on the Continuous Current Tokamak (CCT) in which transport barriers were generated by directly driving edge flow using torque due to radial currents driven by biased electrodes [4]. Biasing has been used to produce improved confinement in a number of subsequent experiments including toroidal devices [5–7, 24, 25] and linear magnetized plasmas [8–10]. Turbulence can self-regulate through the generation of flows and flow shear (zonal flows) [2]; direct evidence for turbulent-Reynolds-stress-driven flow has been reported in a cylindrical magnetized plasma device [29].

While ample evidence for transport reduction in the presence of sheared flow exists [11, 12] and significant effort and progress has been made in developing a theoretical understanding of the interaction between sheared flow and turbulence, there are still a number of open questions that can be answered by experiment. In particular, the exact mechanism behind turbulence modification and transport suppression by shear is still subject to debate: theories present a number of mechanisms including radial decorrelation [13], nonlinear reduction of turbulent amplitude [14], and modification of turbulent cross-phase [15]. Evidence for all of these mechanisms exists in experimental data [12, 24], but a comprehensive experimental dataset establishing in detail the parameter regimes where each mechanism is important has not been acquired. In part, this is due to the fact that most datasets on flow-turbulence interaction come from studies of spontaneously generated flow or in cases where precise external control over flow and flow shear is not possible. A number of basic plasma experiments have utilized biasing techniques to drive flow and flow shear to study flow driven instabilities (e.g. [16, 17]); however, experiments have not been done in which precise external control over flow shear has been achieved in higher-density plasmas with drift-wave turbulence to systematically study the changes in turbulence characteristics and transport.

In this letter, we report on the first experiments in which external control of flow is used to document the response of turbulence and transport to a continuous variation of flow shear, including a zero shear state and a reversal of the flow direction. Shearing rates

($\gamma_s = \partial V_\theta / \partial r$, where $V_\theta = E_r / B$) from zero to up to five times the turbulent autocorrelation rate measured at zero flow shear (τ_{ac}^{-1}) are achieved; thus, a high resolution scan in both the weak shear regime, $\gamma_s < \tau_{ac}^{-1}$, and the strong shear regime, $\gamma_s > \tau_{ac}^{-1}$ is made. Turbulent particle flux is reduced with increasing shearing rate, regardless of the direction of the flow or sign of the flow shear, with significant reduction occurring for $\gamma_s \sim \tau_{ac}^{-1}$. The observed reduction in particle flux is dominated by a decrease in low-frequency ($f < 10\text{kHz}$) density fluctuation amplitude. For low frequency fluctuations, the crossphase between density and azimuthal electric field fluctuations remain near zero for all shearing rates. With higher shear ($\gamma_s > \tau_{ac}^{-1}$) we observe the emergence of a coherent mode localized spatially in the region of strong flow. Fluctuations from this mode appear to increase density fluctuations above 10kHz, but do not appear to contribute to particle flux.

The Large Plasma Device [18] (LAPD) is a 17m long, $\sim 60\text{cm}$ diameter cylindrical plasma produced by a barium-oxide coated nickel cathode. In the experiments reported here, a plasma of density $\sim 2 \times 10^{12} \text{ cm}^{-3}$ and peak temperature of 8eV is produced in a uniform solenoidal magnetic field of 1000G. The large length of LAPD allows for perpendicular losses to compete with parallel losses resulting in appreciable plasma density in the device edge. Gradients in temperature and density can drive resistive drift-Alfven waves in the edge [30], likely contributing to edge turbulence, though flow instabilities can be present as well [27, 28]. Measurements of electron density, electron temperature, and potential (both plasma potential and floating potential) are made using Langmuir probes. Measurements of ion saturation current ($I_{\text{sat}} \propto n_e \sqrt{T_e}$) and floating potential (V_f) are taken with a 9-tip Langmuir probe (flush-mount tantalum tips) while temperature and plasma potential are determined using a swept Langmuir probe. I_{sat} fluctuations are taken as a proxy for density fluctuations for the measurements reported in this work. Density profiles are determined by scaling averaged I_{sat} profiles to line-averaged interferometer measurements of density. Turbulent particle flux $\Gamma \propto \langle \tilde{n}_e \tilde{E}_\theta \rangle$ is determined through correlating density fluctuations from one tip of this probe with azimuthal electric field fluctuations (E_θ) derived from floating potential fluctuations on two azimuthally separated tips. While electron temperature gradients do exist in the edge region, temperature fluctuation contributions to the measurement of electric field are difficult to quantify; it is assumed here that the small tip separation helps minimize any slight differences in temperature and that floating-difference measurements are sufficient. Azimuthal $E \times B$ flow is computed using the swept-probe-derived plasma potential. Flows

derived using this technique compare very well to measurements using Mach probes [9] and flows derived from time-delay estimation (TDE) of the velocity of turbulent structures [19].

Biasing experiments have been previously conducted on LAPD in which edge profile steepening and a reduction in turbulent flux was observed [9, 10]. In these experiments, edge flow was driven by biasing the vacuum chamber wall with respect to the plasma source cathode. Transport reduction occurred only for biases above a threshold value. Below the threshold, azimuthal flow was localized near the biased wall and no flow or flow shear was driven in the region where drift wave turbulence exists. Above the threshold, the flow was able to penetrate radially inward; hence, strong flow and flow shear, with shearing rates far above the low-flow turbulent autocorrelation rate, was driven in the region of strong density gradient. Recent experiments were successful in achieving more continuous control of potential and cross-field flow in the shadow of a small biased obstacle inserted into the LAPD core plasma [20]. Both confinement improvement and degradation (formation of strong density depletions) were observed with the density profile created by the obstacle in this case.

Motivated by the success of biasing obstacles to control flow, a large annular aluminum limiter was installed in LAPD. The limiter provides a parallel boundary condition for the edge plasma and is biased relative to the cathode of the plasma source to control plasma potential and cross-field flow. The limiter is an iris-like design with four radially movable plates located 2.5m from the cathode as shown schematically in Fig. 1(a). The limiters create a 52cm diameter aperture; downstream of the limiter, plasma on field lines with radial location $r > 26\text{cm}$ has the limiter as a conducting end parallel boundary condition and plasma on field lines for $r < 26\text{cm}$ has the anode/cathode of the source region as a parallel boundary condition. An electrically floating conducting end mesh terminates the plasma on the far end of the device. A capacitor bank and transistor switch supply a voltage pulse to the limiter. The bias pulse lasts 5ms during the flat-top of the $\sim 15\text{ms}$ plasma discharge. The limiter is biased from $\sim 10\text{V}$ below to 50V above the anode potential. Typically, plasma potential in the core LAPD plasma (plasma on field lines that connect to the source region) is very close to the anode voltage and the cathode sits near ground (vacuum chamber wall). The anode potential is above the cathode potential by the discharge voltage, which was $\sim 40\text{V}$ during these experiments.

Spontaneous azimuthal rotation of the LAPD plasma is observed when the limiters are

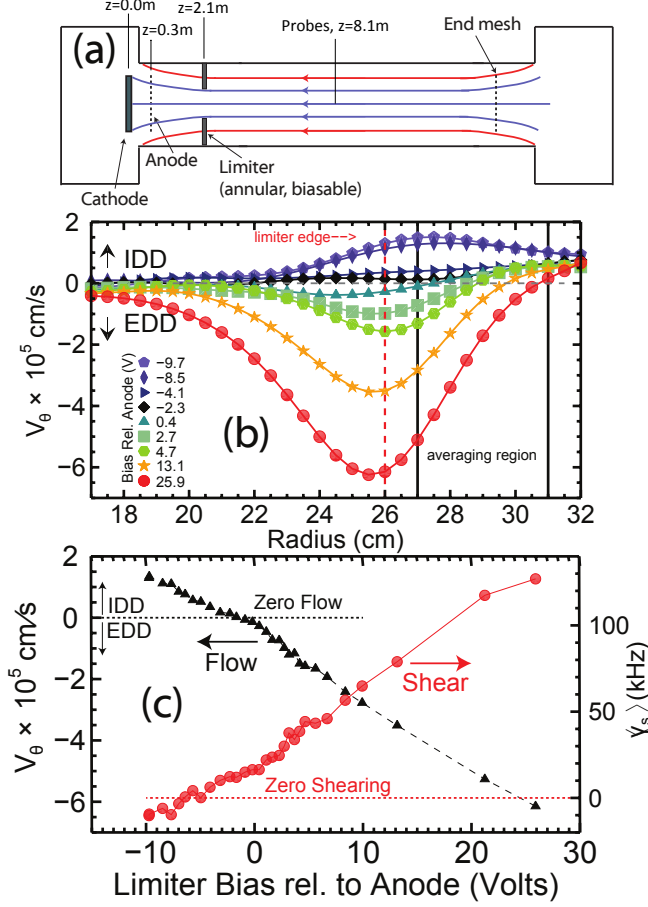


FIG. 1: (a) Diagram of the LAPD device showing axial position of cathode, anode, annular limiters, and Langmuir probes. (b) Velocity profiles using plasma potential from swept measurements. (c) Flow at the limiter edge (black, triangles) and mean shearing rate, averaged over $27 < r < 31 \text{ cm}$ (red, circles).

unbiased (here the limiters are observed to float to a potential $\sim 10 \text{ V}$ below the anode). In this state, an edge flow (peaked just outside the limiter edge) is observed in the ion diamagnetic drift direction (IDD), as shown in Figure 1(a). Biasing the limiter positively with respect to the cathode tends to drive flow in the electron diamagnetic drift direction (EDD). As the limiter bias is increased, the flow in the IDD is first reduced, then brought to separate near-zero flow and zero flow-shear states, and ultimately reversed with strong EDD flow. The ability to zero the flow is of significant importance as the origins of spontaneously-driven/zonal flow can be studied in the context of azimuthal momentum balance [29] given the ability to control how much torque (injected current) is applied to the machine. However, such studies on LAPD deserve a dedicated paper and thus it suffices to report the achievement of such a flow state.

Measurements of profiles of density and particle flux were made for each bias flow state. Values are averaged over a range from $r = 27\text{cm}$ to $r = 31\text{cm}$, a region where average flow and flow shear scale nearly linearly with limiter bias, as shown in Figure 1(b). All other quantities shown in this paper are spatially-averaged over the same region.

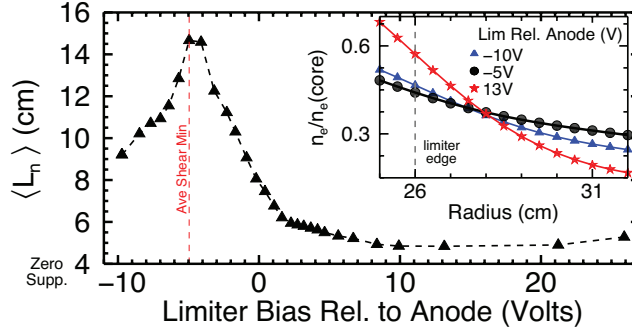


FIG. 2: Density gradient length scale versus limiter bias. Inset shows density profile at three bias values.

Figure 2 shows the variation in the spatially-averaged density gradient length scale, $L_n = |\nabla \ln n|^{-1}$ with increasing limiter bias. As the limiter bias is increased, reducing the IDD flow, an increase in the gradient scale length is observed, indicating a degradation of radial particle confinement. The gradient scale length peaks when the averaged shearing rate is near zero. As the bias is increased further, reversing the flow and again increasing the shearing rate, the gradient gradually steepens and the scale length is lowered, indicating improved radial particle confinement.

The observed variation of $\langle L_n \rangle$ with bias is best organized when compared to the shearing rate, γ_s , as is shown in Figure 3(a). The shearing rate is normalized to the autocorrelation rate of density fluctuations measured in the zero-shear state. An autocorrelation rate of $\tau_{ac}^{-1} \approx 28\text{kHz}$ ($\tau_{ac} \approx 36\mu\text{s}$) is calculated by taking the half-width at half-maximum of a Hilbert transform of the I_{sat} autocorrelation function. Confinement improvement (decreased $\langle L_n \rangle$) occurs continuously and gradually with increasing γ_s and reaches saturation for $\gamma_s \approx \tau_{ac}^{-1}$ (a normalized γ_s of 1). The profile steepening appears to be largely independent of the direction of the flow (or radial electric field): IDD (filled points) and EDD (open points) flow cases follow the same trend when plotted against normalized shearing rate.

Measured changes in turbulence and turbulent particle flux are consistent with the ob-

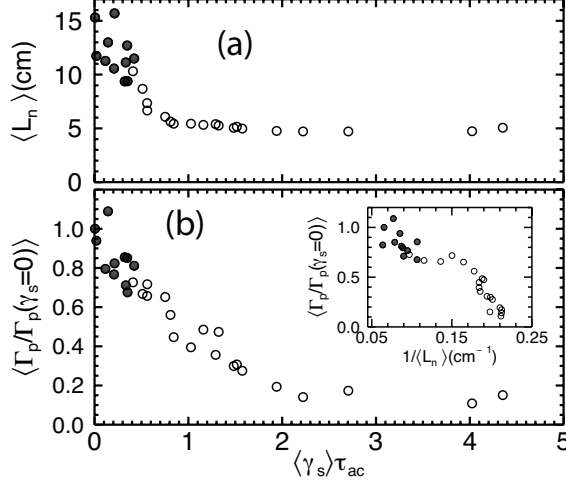


FIG. 3: (a) Gradient scale length versus shearing rate. (b) Particle flux normalized to no-shear flux as a function of normalized shearing rate. Filled symbols represent points with flow in the IDD. Inset: Measured turbulent particle flux versus gradient scale length.

served changes in the density profile. The turbulent particle flux can be written[21]:

$$\Gamma = \frac{2}{B} \int_0^\infty |n(f)| |E_\theta(f)| \gamma_{(n,E_\theta)}(f) \cos[\phi_{(n,E_\theta)}(f)] df \quad (1)$$

where $n(f)$ and $E_\theta(f)$ are the Fourier transforms of the density and azimuthal electric field fluctuations; $\gamma_{(n,E_\theta)}$ is the coherency between density and electric field; and $\phi_{(n,E_\theta)}$ is the cross-phase angle between density and electric field.

Figure 3(b) shows the spatially-averaged turbulent particle flux as a function of normalized shearing rate. The turbulent flux decreases continuously with increasing shearing rate; however the observed decrease is slightly slower than that observed for L_n . The inset in Figure 3(b) shows that the variation in turbulent flux is correlated with the changes in L_n (but scales in a way that is inconsistent with Fick's law using a fixed diffusion coefficient). The trend in reduced particle flux is the same for either direction of flow (IDD or EDD). The cause for the reduction in turbulent particle flux can be explored by considering individual terms in the integrand of Eqn. 1.

Density fluctuations were reduced significantly with increasing shearing in these experiments. Figure 4(a) shows changes in the spatially-averaged density fluctuation spectrum with shearing rate. The shearing rate is signed in this figure, and negative shearing rates occur for flow in the IDD. Most of the power is located in frequencies $< 10\text{kHz}$ and in this range, power decreases overall with increasing shearing rate. A decrease of about one order of magnitude in fluctuation power is seen between the minimum shear state and the high

shear regime where L_n and particle flux are minimized; this is made clearer in Figure 4(b). At higher shearing rates, $\gamma_s \gtrsim \tau_{ac}^{-1}$, a coherent mode emerges. The frequency of the mode increases with shearing rate and the fluctuation amplitude is localized to the peak of the azimuthal flow.

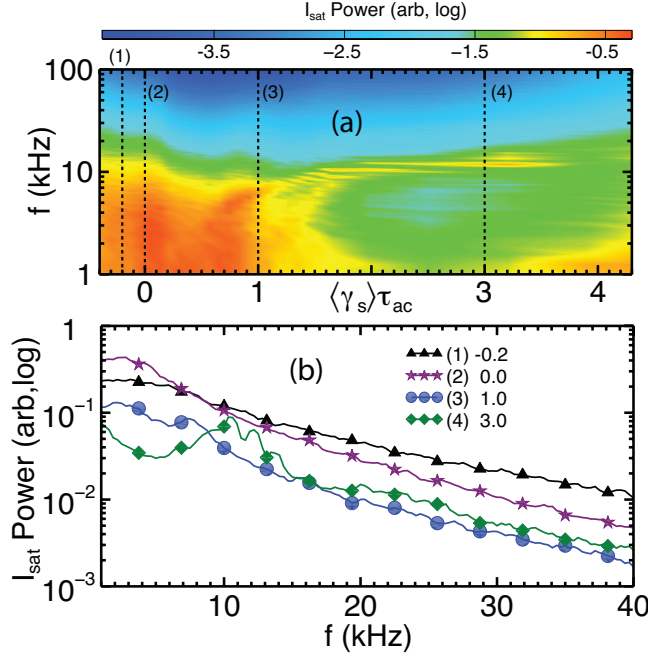


FIG. 4: (a) Contour plot of $\log I_{sat}/\text{density fluctuation power}$ versus shearing rate and frequency. (b) Power spectra for four different values of shearing rate.

Figure 5(a) shows the reduction in total density fluctuation amplitude with shear in two frequency bands: all frequencies below 100kHz in black and all frequencies above 10kHz in red. With the emergence of the coherent mode, the high frequency fluctuation amplitude does show an increasing trend at higher shearing rates but there is a strong overall decrease in fluctuation amplitude with shearing. A reduction is also seen in E_θ fluctuation amplitude, as shown in Figure 5(b); however this reduction is weaker than observed in density fluctuations. The cross-phase between n and E_θ does not change significantly with shearing. As shown in Figure 5, $\cos[\phi_{(n,E_\theta)}] \sim 1$ for all shearing rates. For higher frequencies ($f > 10\text{kHz}$), the cross-phase does change with shearing, with $\cos[\phi_{(n,E_\theta)}]$ trending toward zero at higher shear. This crossphase change explains why the coherent mode that emerges at higher shearing rate does not contribute to an increase in the particle flux. The coherency between n and E_θ also decreases with shearing rate, as shown in Figure 5. Overall, the de-

crease in flux is primarily due to a decrease in turbulent amplitude. This observation is distinct from previous work with flows driven by vacuum-chamber-wall biasing on LAPD. In those experiments, turbulent amplitude decreased little while the turbulent cross-phase experienced a significant change, leading to reduced particle flux [10]. In the experiments reported here, the magnetic field is higher (1000G versus 400G) and normalized shearing rates are lower (near unity). Cross-phase change is expected in cases with very strong shearing ($\gamma_s \gg \tau_{ac}^{-1}$) [22]. Future experiments will explore the variation of the turbulent response to higher normalized shearing through changing plasma parameters, in particular magnetic field.

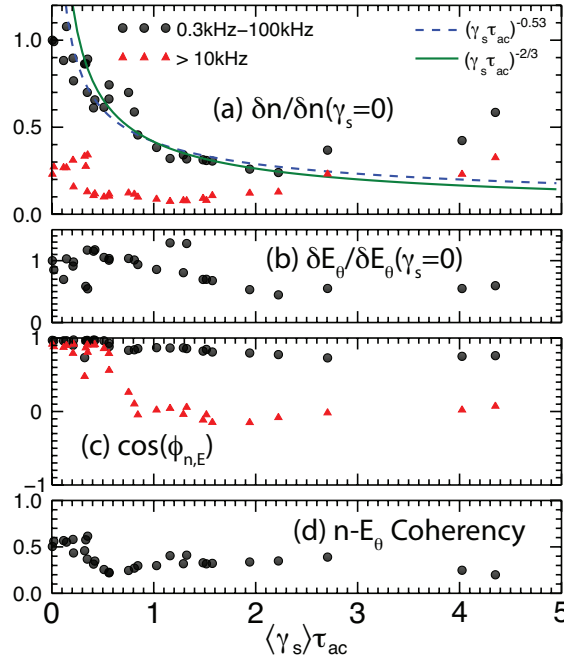


FIG. 5: Components of particle flux versus shearing rate including I_{sat} /density fluctuation power(a), electric field fluctuation power(b), crossphase(c) and coherency(d) with black points for low or all frequency, red for high only.

Lastly, we add a comparison of our data to a simple theory, the Biglari-Diamond-Terry (BDT) model [13], which predicts a power-law scaling with shearing rate of the turbulent amplitude of the form: $(\gamma_s/\tau_{ac}^{-1})^{-\alpha}$. As seen in Figure 5, a best fit of $\alpha = 0.530$ compares favorably to the BDT prediction of $\alpha = 2/3$ for the reduction in density fluctuation amplitude. It should be noted, however, that the BDT model is fairly simple and the validity of its assumptions is questionable for the experimental conditions reported here. In particular, as

the shearing rate is increased in LAPD, the density profile is changing (in BDT a fixed drive is considered). Future work will focus on direct comparisons to more comprehensive models of shear suppression, including comparisons to two-fluid simulations using the BOUT++ 3D turbulence code [23].

This letter presents the first experiments in which the response of pressure-gradient-driven turbulence to a continuous variation of shearing rate, including a zero flow state, a near-zero flow shear state and a reversal in the direction of flow, is studied. Increased shearing improves radial particle confinement regardless of the direction of the azimuthal flow or sign of the flow shear. The observed reduction of turbulent particle flux with shear is attributed to a reduction in the amplitude of density fluctuations. These experiments were performed at a fixed set of plasma parameters (fixed magnetic field, neutral pressure, discharge power); future work will explore the variation in turbulent response to shear as these parameters are varied as well as a more detailed analysis of the zero-flow state.

-
- [1] K. Burrell, Phys. Plasmas **4**, 1499 (1997).
 - [2] P. Terry, Rev. Mod. Phys. **72**, 109 (2000).
 - [3] F. Wagner *et al.*, Phys. Rev. Lett. **49**, 1408 (1982).
 - [4] R. Taylor *et al.*, Phys. Rev. Lett. **63**, 2365 (1989).
 - [5] R. Weynants *et al.*, Nucl. Fusion **32**, 837 (1992).
 - [6] J. Boedo *et al.*, Nucl. Fusion **40**, 7 (2000).
 - [7] C. Silva *et al.*, Plas. Phys. Control Fusion **48**, 727 (2006).
 - [8] O. Sakai and Y. Yasaka and R. Itatani, Phys. Rev. Lett. **70**, 4071 (1993).
 - [9] J. Maggs *et al.*, Phys. Plasmas **14**, 052507 (2007).
 - [10] T. Carter and J. Maggs, Phys. Plasmas **16**, 012304 (2009).
 - [11] K. Burrell, Phys. Plasmas **6**, 12 (1999).
 - [12] G. Tynan *et al.*, Plasma Phys. Control Fusion **51**, 113001 (2009).
 - [13] H. Biglari *et al.*, Phys. Fluids B. **2**, 1 (1990).
 - [14] E.-J. Kim *et al.*, Phys. Plasmas **11**, 10 (2004).
 - [15] A. Ware *et al.*, Plasma Phys. Control Fusion **38**, 1343 (1996).
 - [16] W.E. Amatucci *et al.*, Phys. Rev. Lett. **77**, 1978 (1996).

- [17] D. Jassby, Phys. Fluids **15**, 9 (1972).
- [18] W. Gekelman *et al.*, Rev. Sci. Instrum. **62**, 2875 (1991).
- [19] C. Holland *et al.*, Rev. Sci. Instr. **75**, 10 (2004).
- [20] S. Zhou *et al.*, Phys. Plasmas **19**, 012116 (2012).
- [21] E. Powers, Nucl. Fusion **14**, 749 (1974).
- [22] P.W. Terry and D.E. Newman and A.S. Ware, Phys. Rev. Lett. **87**, 185001 (2001).
- [23] M. Umansky *et al.*, Phys. Plasmas **18**, 055709 (2011).
- [24] J.A. Boedo *et al.*, Nucl. Fusion, **42**, 177-121 (2002).
- [25] P. Peleman *et al.*, J. Nucl. Fusion Mat., 363-365 (2007) 638-642.
- [26] F. Wagner, Plasma Phys. Control Fusion **49** B1-B33 (2007)
- [27] W. Horton *et al.*, Phys. Plasmas, **12**, 022303 (2005)
- [28] P. Popovich *et al.*, Phys. Plasmas, **17**, 102107 (2010)
- [29] C. Holland *et al.*, Phys. Rev. Lett., **96**, 195002, (2006)
- [30] J.E. Maggs and G.J. Morales, Phys. Plasmas, **10**, 6, (2003)